Reliability-Based Optimal Design and Tolerancing for Multibody Systems Using Explicit Design Space Decomposition

Henry Arenbeck
RWTH-Aachen University,
Institute of Automatic Control,
52074 Aachen, Germany
e-mail: h.arenbeck@irt.rwth-aachen.de

Samy Missoum
e-mail: smissoum@email.arizona.edu

Anirban Basudhar
e-mail: anirban@email.arizona.edu

Parviz Nikravesh
e-mail: pen@email.arizona.edu

Department of Aerospace and Mechanical Engineering,
University of Arizona,
Tucson, AZ 85721

This paper introduces a new approach for the optimal geometric design and tolerancing of multibody systems. The approach optimizes both the nominal system dimensions and the associated tolerances by solving a reliability-based design optimization (RDBO) problem under the assumption of truncated normal distributions of the geometric properties. The solution is obtained by first constructing the explicit boundaries of the failure regions (limit state function) using a support vector machine, combined with adaptive sampling and uniform design of experiments. The use of explicit boundaries enables the treatment of systems with discontinuous or binary behaviors. The explicit boundaries also allow for an efficient calculation of the probability of failure using importance sampling. The probability of failure is subsequently approximated over the whole design space (the nominal system dimensions and the associated tolerances), thus making the solution of the RBDO problem straightforward. The proposed approach is applied to the optimization of a web cutter mechanism. [DOI: 10.1115/1.4000760]

Keywords: multibody systems, tolerancing, uncertainty, reliability-based design optimization, support vector machines, design of experiments

1 Introduction

It is well known that tolerances, which determine the acceptable range of geometric uncertainty, can have a significant impact on the properties of multibody systems. Too large tolerances can trigger unwanted behaviors and lead to the reduction in system reliability [1,2]. Too narrow tolerances result in an unnecessarily high technological effort for manufacturing and high production costs. Numerical models of complex multibody systems are usually based on deterministic geometric parameters. However, when uncertainty is considered, these parameters are randomly distributed within tolerance intervals. If the distributions are known, it is possible, in theory, to propagate the uncertainties and find the corresponding distribution of responses of the system.

Several methods exist to propagate uncertainties and estimate, for instance, a probability of failure. The most used and basic approach is based on the Monte-Carlo simulations (MCS), which typically requires a very large number of "tests" of system realizations to obtain an estimate of the probability of failure. For efficiency, MCS are often coupled with a response approximation (e.g., a response surface or metamodel [3,4]), which enables large amounts of samples without repetitive calls to often expensive function evaluations. However, there is obviously a strong dependency of the estimated probability of failure on the quality of the response approximation. Moment-based approaches, such as first and second-order reliability methods (FORM and SORM) [5], stem from another class of techniques, which are based on a linear or quadratic approximation of the limit state function (boundary of the failure domain). These approaches often lack accuracy for a complex failure domain (e.g., disjoint failure spaces or highly nonlinear limit state functions). A more general tool is provided by polynomial chaos expansion (PCE), which enables the propagation of uncertainties of known probabilistic distributions to obtain the corresponding distribution of a response [6]. All the aforementioned methods present limitations for problems with large computational times per simulation and highly nonlinear behaviors (e.g., discontinuous responses). Uncertainty propagation techniques are also used in association with optimization techniques for robust design or reliability-based design optimization (RBDO). These methods have been applied to many problems in aerospace and mechanical engineering [7–10]. However, their application to multibody systems is, to the best of the authors' knowledge, rare.

This article proposes a novel methodology for the optimal geometric design of multibody systems with consideration of geometric uncertainty. The method is based on the notion of explicit design space decomposition, whereby the boundaries of failure regions (i.e., regions that are associated to unacceptable system performance) are defined explicitly as a function of the geometric characteristics of the system. This decomposition is created using a machine learning technique referred to as support vector machines (SVMs) [11], uniform design of (computer) experiments (DOEs) [12,13], and adaptive sampling. The construction of explicit limit state functions using SVMs present the following advantages.

- It enables a straightforward use for MCS-based estimation of the probability of failure while avoiding computationally expensive multibody simulations. The SVM-based approach can generate disjoint and nonconvex failure regions.
- It can handle discontinuous responses and binary design problems (e.g., pass or fail). These problems are not treatable using traditional response surface/metamodel approaches, which approximate the responses.
- It provides a framework for adaptive sampling and reduces the number of computationally intensive function calls [14,15].
- Once the explicit limit state function is created, it is possible to perform a reliability-based design optimization quite efficiently [16–18].

Contributed by the Design for Manufacturing Committee of ASME for publication in the Journal of Mechanical Design. Manuscript received January 30, 2009; final manuscript received November 16, 2009; published online February 9, 2010. Assoc. Editor: Michael Kokkolaras.

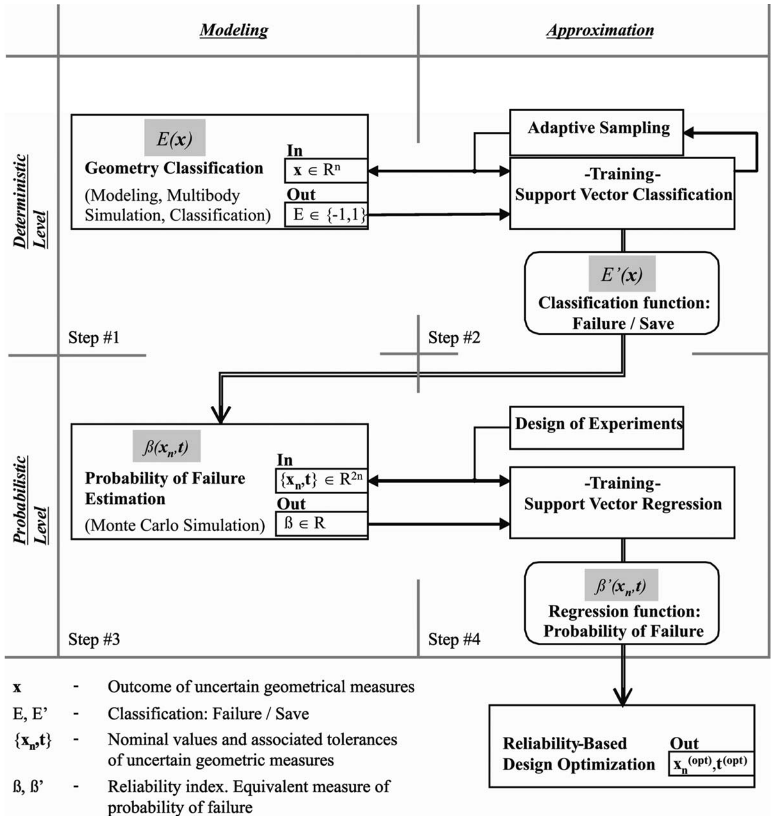

Fig. 1 Overall scheme of geometric design methodology

- It gives the designer more insight into the design space by providing straightforward relationships between regions of the design space and specific mechanical behaviors [17].

In this article, the explicit design space decomposition is applied to the design of a web cutter, for which the member lengths are within some tolerance intervals. A reliability-based design optimization is performed in order to find the optimal nominal geometric configuration and corresponding tolerances that minimize the cost while resulting in a probability of failure lower than a specific target.

2 Methods

The proposed methodology is aimed at generating an explicit analytical function, which maps the probabilistic distribution of the geometric measures of the mechanical system to the resultant probability of failure. This function can be used in the objective or in the constraints of an RBDO problem, allowing the RBDO problem to be solved efficiently. The methodology is based on the modeling of the mechanical system and approximation at the deterministic and the probabilistic level.

The basic steps of the approach are summarized in Fig. 1. Deterministic modeling (step one) refers to the simulation of the mechanical system using fundamental physical relations (first principles). An algorithm is defined that first accepts an arbitrary realization of the uncertain geometric measures, then integrates this realization into the system model and simulates the resultant dynamic system behavior. Finally, the dynamic behavior is categorized as satisfactory or not. In this step, all the specifics concerning the mechanical system are defined (Sec. 2.1).

Deterministic approximation (step two) refers to the construction of an explicit limit state (classification) function. One key feature of the proposed approach stems from the fact that the limit state is constructed using an SVM, which is efficiently evaluated (Sec. 2.2). This is the most delicate step of the methodology as it is imperative to minimize the number of simulation calls, which, in real world applications, may individually require multiple hours of computation. An adaptive sampling technique is employed to minimize the number of simulation calls necessary (Sec 2.3).

Probabilistic modeling (step three) refers to the definition of an algorithm, which accepts the probabilistic distribution of the uncertain geometric measures of the mechanical system and generates an estimate of the resultant probability of failure (i.e., the probability of emergence of unsatisfactory dynamic behavior). The probabilistic distribution is expressed as a function of a finite number of scalar parameters: the nominal geometric measures and the associated tolerances. The probability of failure estimate is obtained by means of MCS. In each MCS-trial, the explicit limit state function is employed (Sec. 2.4), allowing computationally expensive calls of multibody simulations to be avoided. As a result, MCS are computationally feasible even if complex real world problems and high accuracy are considerd.

Probabilistic approximation (step four) refers to the derivation of a regression model that approximates the input-output-relation obtained through MCS (i.e., the relation between the nominal geometric measures along with the associated tolerances and the resultant probability of failure, Sec. 2.4). An RBDO problem, involving the regression model, which does not require calls to multibody simulations or MCS, is then formulated. The problem can be solved efficiently using standard nonlinear optimization methods, while still incorporating a high (theoretically, nearly full) degree of the relevant complexity of both the deterministic and the probabilistic model (Sec. 2.5).

In the following sections, all main components of the described methodology are explained in more detail.

2.1 Multibody Simulation and Classification. In order to apply the proposed methodology to a multibody system, multibody simulation is necessary to verify if a specific realization of the system under consideration (with given fixed geometric characteristics) is acceptable or not. This is essential as the SVM ex-

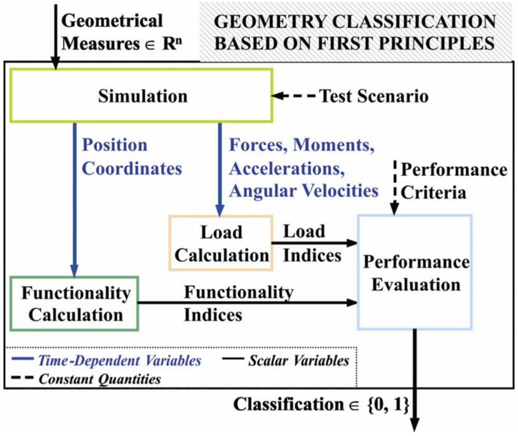

Fig. 2 Basic scheme of geometric configuration classification by means of multibody simulation

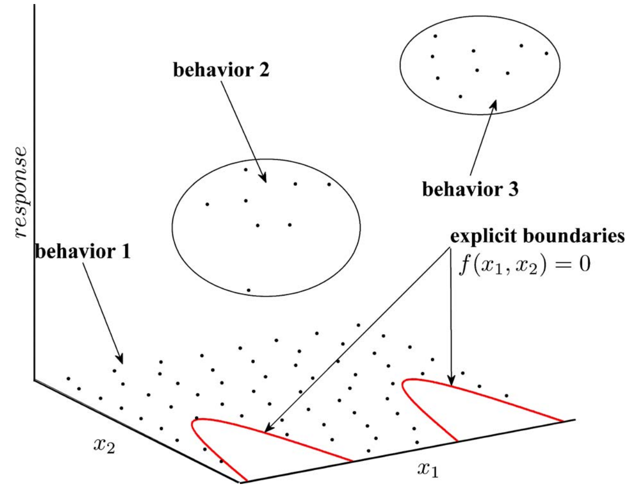

Fig. 3 Example of three "behaviors." Definition of explicit boundaries in the parameter space (x_1, x_2) corresponding to the behaviors.

plicit design space decomposition is based on this binary classification of the geometric realizations. The overall scheme for simulation-based derivation of such classification, referred to as "Geometry Classification", is depicted in Fig. 2.

The geometric configuration to be analyzed is first incorporated into the multibody system model, which is then employed for simulations using predefined representative system excitations. Simulation results are the system responses (forces, velocities, etc.), which are transferred to the load and functionality calculation modules.

The position coordinates, holding the trajectory information of all system components, and hence, characterizing the geometric system component interplay, are processed by the "Functionality Calculation" module, yielding scalar indices that characterize the quality of the geometric system movement. Such quality measure could, for example, be the mean deviation of an end-effector trajectory from the optimal one. The time information is eliminated in this process.

The forces, moments, accelerations, and velocities are transferred to the "Load Calculation" module. There, the normal and shear stresses developed in the system components are computed. These are then transformed into equivalent normal stresses, using an appropriate comparison stress hypothesis. Afterwards, the maximum stresses over space and time are computed for each system component and transferred as load indices to the "Performance Evaluation" module.

In the "Performance Evaluation" module, load and functionality indices are used to classify the system as either failing or not failing by comparing the overall dynamic performance displayed by the performance indices with performance criteria (e.g., maximum allowed stresses). In this work, such criteria are constant quantities, and are defined a priori.

The decision on system performance is the final output of a processing sequence that started with the definition of the target multibody system geometry. The geometry classification module comprising simulation, functionality calculation, load calculation, and performance evaluation, can therefore be interpreted as a classifier that assigns a binary decision to a given outcome of the uncertain geometric system measures, which can be located anywhere inside the "accepted" geometric region defined by the tolerance intervals.

2.2 Design Space Decomposition Using Support Vector Machines. In order to provide a better understanding of the design space and its relation to cost and performance, this work proposes to decompose the design space explicitly with support vector machines [16,18–20]. This novel approach provides a deeper insight into the design space through the association of one type of response with one specific region of the design space. In addition, as one of its most remarkable features, it allows an easy calculation of probabilities of failure. An example of design space decomposition with an SVM is given in Fig. 3. The example shows three response clusters with respect to two variables. The regions of the design space with the highest response are delimited explicitly in terms of the variables using the SVM.

More precisely, consider a system whose responses (or any other quantities such as the cost) have been evaluated based on a design of experiments and classified as acceptable or unacceptable. The responses can then be projected onto the design space to create a mapping between regions of the design space and "clouds of responses" (Fig. 3). Note that, as in the depicted example, the responses might be discontinuous with clouds that are associated with very distinct system behaviors. Using this mapping, the designer can associate changes in the system's characteristic quantities (e.g., performance) with regions of the design space. However, if only a few discrete data points are available, this might not be very useful. For this reason, it is beneficial to obtain an explicit expression of the region boundaries in the design space, such as the ones given by SVMs. In other words, an analytical expression for limit state functions is obtained. This forms the basis of the concept of explicit decomposition of the design space.

Support vector machines, which are traditionally used for the classification of data, provide a natural and powerful tool for the construction of limit state functions. SVMs create a general expression for a function that optimally separates two classes. The SVM value is positive for one class and negative for the other. Based on the SVM value at a point, the confidence of the decision can be evaluated. The general expression of an SVM limit state function is given as:

$$s(\mathbf{x}) = b + \sum_{i=1}^{n_{SV}} \alpha_i y_i K(\mathbf{x_i}, \mathbf{x}) = 0 \tag{2.1}$$

where $\mathbf{x_i}$ are support vectors, $y_i \in \{1,-1\}$ are the class labels, K is a kernel function, b is the bias, and α_i are the Lagrange multipliers associated to the support vectors. The support vectors and the Lagrange multipliers are found through the maximization of the margin, which is the separation between classes $y_i=\text{sign}(s(\mathbf{x_i}))=1$ and $y_i=-1$ in a high dimensional feature space [21]. Several choices can be made for the kernel function like the polynomial and the Gaussian kernel. The Gaussian kernel used in this research is given as:

$$K(\mathbf{x_i}, \mathbf{x}) = e^{-(\|\mathbf{x}-\mathbf{x_i}\|^2/2\sigma^2)} \tag{2.2}$$

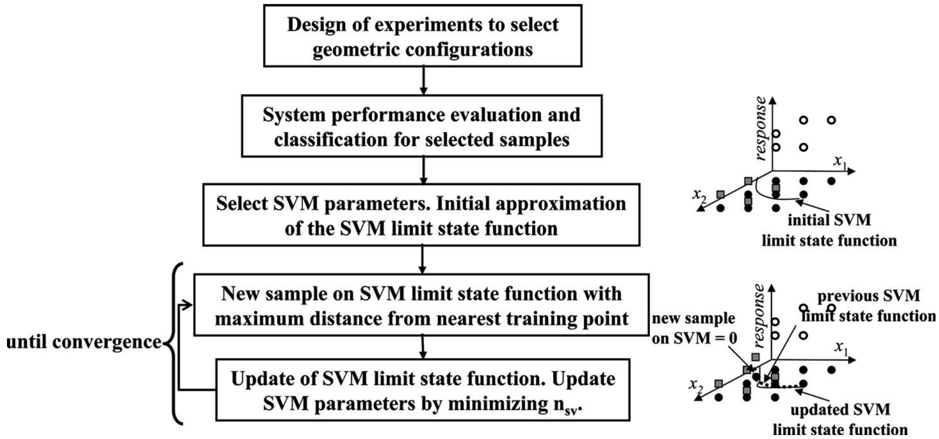

Fig. 4 Adaptive sampling method to construct an SVM limit state function

SVMs are a very general tool, as the limit state function can be nonconvex and form disjoint subregions in a high dimensional space. As classifiers, SVMs are more attractive than neural networks because they provide an explicit limit state function, and overfitting is avoided.

2.3 Adaptive Sampling for Minimal Number of Experiments. In order to reduce computational costs, the number of geometry classifications for constructing the limit state function should be minimized. However, using too few samples can compromise the accuracy of the SVM limit state function. The accuracy of the limit state function depends both on the quantity and the quality of the training samples. Therefore, an adaptive sampling technique is used to reduce the number of samples required to generate an accurate SVM limit state function (Fig. 4).

An initial estimate of the limit state function is made using a reasonably small training set consisting of N_{init} samples. The design of experiments used to select the initial samples should be as uniformly distributed in the space as possible. For this purpose techniques such as centroidal Voronoi tessellations (CVT) [12] can be used. The initial estimate of the limit state function is then refined through the selection of new samples, based on the following criteria [14,15]:

- The samples are added on the limit state function, as the probability of misclassification is highest at this location.
- The new samples are added in the sparsely populated regions of the space.

The above objectives are realized by adding new samples on the limit state function while maximizing the distance to the nearest existing training sample [15]

$$\begin{aligned} &\max_{\mathbf{x},z} \quad z \\ &\text{s.t.} \quad \|\mathbf{x}-\mathbf{x_i}\| \geq z \qquad (2.3) \\ &s(\mathbf{x}) = 0 \end{aligned}$$

The SVM limit state function is updated by adding new samples according to the above criteria until a stopping criterion is met [14]. The SVM kernel parameters are updated after each sample evaluation by minimizing the number of support vectors n_{SV}.

2.4 Probability of Failure. The probability of occurrence of a nonacceptable system performance, referred to as probability of failure, is defined as

$$p_f(\mathbf{x_n},\mathbf{t}) = \int_{\Omega_f} f_{\mathbf{X}}(\mathbf{x};\mathbf{x_n},\mathbf{t})d\mathbf{x} \qquad (2.4)$$

where $f_{\mathbf{X}}(\mathbf{x};\mathbf{x_n},\mathbf{t})=\Pi_{k=1}^{nv} f_{x_k}(x_k;x_k^{(n)},t_k)$[1] is the joint probability density function (PDF) of the random geometric measures $\mathbf{x}=[x_1 \ x_2 \ \ldots \ x_{nv}]^T$. This function characterizes the random process that generates different outcomes of the target multibody system. The nominal geometric measures $\mathbf{x_n}=[x_1^{(n)} \ x_2^{(n)} \ \ldots \ x_{nv}^{(n)}]^T$ and the corresponding tolerances $\mathbf{t}=[t_1 \ t_2 \ \ldots \ t_{nv}]^T$ determine the intervals of the distributions of geometric measures:

$$x_k^{(n)} - t_k \leq x_k \leq x_k^{(n)} + t_k$$

$$f_{x_k}(x_k)\begin{cases} \neq 0 & x_k \in [x_k^{(n)} - t_k, x_k^{(n)} + t_k] \\ =0 & \text{otherwise} \end{cases} \qquad k \in \{1,2,\ldots,nv\} \qquad (2.5)$$

The integration domain Ω_f in Eq. (2.4) is the subspace of all nonacceptable geometric configurations—the failure domain.

Assuming that:

- the joint PDF $f_{\mathbf{X}}(\mathbf{x};\mathbf{x_n},\mathbf{t})$ can be determined a priori for any configuration of nominal geometric measures $\mathbf{x_n}$ and associated tolerances $\mathbf{t}$; and
- the boundary of the failure domain (the limit state) can be described as a function of the geometric measures, $g(\mathbf{x})=0$;

the probability of failure can be estimated using a FORM/SORM [5] or another technique such as the advanced mean value (AMV) method [22]. Such methods may be inappropriate in the case of a multibody system whose responses might be discontinuous with highly nonlinear limit state functions, sometimes representing the boundaries of disjoint failure domains.

MCS offers an alternative way of estimating the solution of Eq. (2.4). The basic idea of MCS is to create multiple realizations $\mathbf{x}$ of the random process characterized by $f_{\mathbf{X}}(\mathbf{x};\mathbf{x_n},\mathbf{t})$, and to classify each realization as either failure (unacceptable system performance) or safe (acceptable system performance). Hence, the real world random process that generates either functioning or failing systems is replicated, and a great amount of virtual empirical data is created. From these data, the probability of emergence of nonacceptable system performance can be estimated as

$$\tilde{p}_f(\mathbf{x_n},\mathbf{t}) = \frac{N_f(\mathbf{x_n},\mathbf{t})}{N} \qquad (2.6)$$

[1] Assuming statistical independence of all geometric measures.

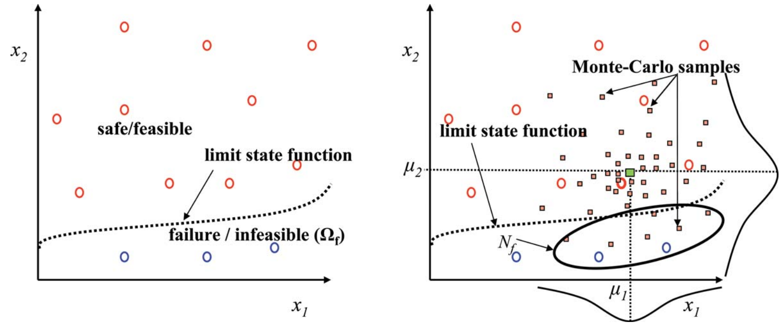

Fig. 5 Explicit failure region boundary constructed with an SVM (left), and MCS (right). Example with two random variables x_1 and x_2 with means μ_1 and μ_2.

where $N_f(\mathbf{x_n},\mathbf{t})$ is the number of realizations $\boldsymbol{x}$ that were classified as failure and N is the total number of realizations created. The main advantages of MCS are its simplicity and generality: MCS can be implemented easily and any distribution of the geometric measures can be processed.

It can be shown that the maximum relative error of MCS-based probability of failure estimation, within a 95% confidence interval, is equal to [5]:

$$\varepsilon = \frac{\tilde{p}_f - p_f}{p_f} = 2\sqrt{\frac{(1-p_f)}{Np_f}} \approx 2\sqrt{\frac{1}{N_f}} \tag{2.7}$$

As expected, the relative error decreases as N increases. Also, the error can become large for very small values of p_f. Hence, if the probability of nonacceptable system performance is small, as is the usual case when dealing with geometric tolerances, traditional MCS requires evaluation of a large number of trials in order to obtain accurate results.

The efficiency of MCS can be improved in two ways as follows:

- Reduction in the number of trials required for a given accuracy.
- Reduction in the computational cost of each individual trial.

The first point is addressed using variance reduction techniques such as importance sampling and stratified sampling [5]. Importance sampling, in a simple form, can be implemented efficiently. It allows setting up freely the joint PDF to be employed in MCS for the generation of geometric realizations. Using this function, $f_{\mathbf{x}}^{(\mathrm{bias})}(\mathbf{x};\mathbf{x_n},\mathbf{t})$, referred to as the biasing function, and the real PDF of the actual process $f_{\mathbf{X}}(\mathbf{x};\mathbf{x_n},\mathbf{t})$, the probability of failure is:

$$\tilde{p}_f(\mathbf{x_n},\mathbf{t}) = \frac{1}{N}\sum_{k=1}^{N} e(\mathbf{x_k})\frac{f_{\mathbf{X}}(\mathbf{x_k};\mathbf{x_n},\mathbf{t})}{f_{\mathbf{x}}^{(\mathrm{bias})}(\mathbf{x_k};\mathbf{x_n},\mathbf{t})},$$

$$e(\mathbf{x_k}) = \begin{cases} 0 & \mathbf{x_k} \in \text{safe region} \\ 1 & \mathbf{x_k} \in \text{failure region} \end{cases} \tag{2.8}$$

The second point is tackled through the use of an explicit limit state function $g(\mathbf{x})$ constructed using an SVM. In this case, the classification of a geometric configuration consists of checking the sign of $g(\mathbf{x})$, which has the form of a series expansion. Thus, a high number of trials can be realized with a reasonable computational cost. Figure 5 shows an example of MCS using a limit state function, which is approximated by an SVM.

2.5 RBDO. The RBDO problem can be stated as follows:

$$\min_{\mathbf{x}_n,\mathbf{t}} \quad F(\mathbf{x_n},\mathbf{t})$$

$$\text{s.t.} \quad p_f(\mathbf{x_n},\mathbf{t}) = P(g(\mathbf{x}) \le 0) \le p_{f,\mathrm{target}} \tag{2.9}$$

where F is the objective function and g is a limit state or performance function. The limit state equation $g(\mathbf{x})=0$ divides the space of uncertain geometric measures into a failure region $(g(\mathbf{x})\le 0)$ and a safe region $(g(\mathbf{x})>0)$. $p_{f,\mathrm{target}}$ is the target probability of failure and $\mathbf{x}$ is the vector of a geometric realization. The random quantities are drawn from the interval that is defined by the nominal geometric values $\mathbf{x_n}$ and the corresponding tolerance assignments $\mathbf{t}$. Note that there can be several limit state functions for the same system, each related to a different failure mode.

As mentioned in the previous paragraph, the probability of failure can be evaluated using Monte-Carlo simulations. However, the inclusion of a Monte-Carlo process within an optimization loop is not recommended for three main reasons:

- It is time consuming;
- The probability calculated by Monte-Carlo simulations is noisy due to the randomness of the sampling; and
- The probabilities are typically low and can vary by orders of magnitude during the optimization process.

In order to regularize the probabilistic constraint, the reliability index β is used as a substitute for the probability of failure:

$$\beta = -\Phi^{-1}(p_f) \tag{2.10}$$

where Φ is the standard normal cumulative density function.

The optimization problem is then rewritten as:

$$\min_{\mathbf{x}_n,\mathbf{t}} \quad F(\mathbf{x_n},\mathbf{t})$$

$$s.t. \quad \beta_{\mathrm{target}} - \beta(\mathbf{x_n},\mathbf{t}) \le 0 \tag{2.11}$$

In order to improve computational efficiency, the reliability index is approximated by a regression function. This is done by first generating a uniform DOE in a space spanned by the nominal dimensions and the associated tolerances. MCS are run for each sample, thus providing the corresponding probability of failure. The purpose of this first DOE is to identify the region (a hyper rectangle) of the space where the probability of failure is smaller than a given value (which is larger than the target probability of failure used in the RBDO problem). In this subspace, a second DOE is performed and the reliability index obtained via MCS is approximated by a support vector regression (SVR) [23] function based on a Gaussian kernel.

3 Application Example

The proposed optimization scheme was applied to a web cutter mechanism. Uncertain geometric measures are assumed to be the distances Q-A (denoted as x_1), A-B (denoted as x_2), and B-O (denoted as x_3), as depicted in Fig. 6. The performance of the web cutter mechanism depends strongly on these measures. In the following sections, specific details of all previously described tech-

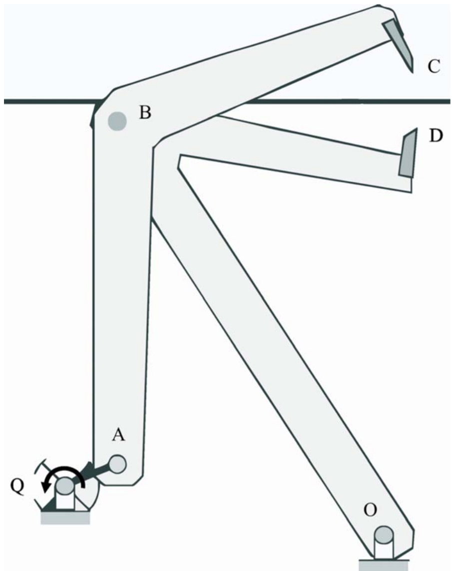

Fig. 6 Sketch of a simplified web cutter mechanism

niques are presented, ultimately allowing for a probabilistic optimization of the geometric configuration of the web cutter mechanism. The application example is aimed at illustrating the presented concepts. As a result of some simplifications of real world physical relations, practical applicability cannot be expected.

3.1 Multibody Simulation. The web cutter was modeled as a planar mechanism consisting of five rigid bodies. A schematic picture of the mechanism is given in Fig. 7. Only revolute joints and rigid joints are present in the model. Bodies 1 and 3 are connected to the ground through revolute joints at points Q and O. A revolute joint at point A connects bodies 1 and 2, and another revolute joint at point B connects bodies 2 and 3. Two rigid joints at point B connect bodies 2 and 4, and bodies 3 and 5, respectively. All bodies are assumed to be beams of constant density and constant cross section.

A body coordinate formulation is used, whereby all employed mathematical relations are expressed in terms of coordinates, which uniquely define the location of each individual body in two-dimensional space [24]. An inverse simulation of the web cutter dynamic behavior is performed, providing the angular coordinate of body 1 ϕ_1 as motion input [24]. The reaction forces at each joint are extracted [24]. The only external forces considered are the web resistance forces. They are applied at points C and D, once the cutting event is detected. The magnitude of these forces is assumed to be constant.

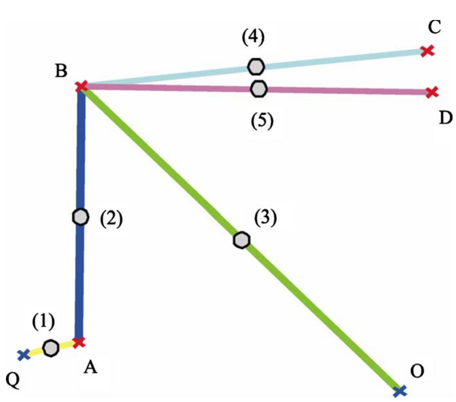

Fig. 7 Multibody model of a web cutter mechanism

The simulation scenario is defined by the motion input $\phi_1(t)$. This input imposes a predefined angle, zero angular velocity, and zero angular acceleration on body 1 at time step one. Over a predefined initial time period, the angular velocity is smoothly increased to a target value. After that, it is held constant. Simulation is performed until body 1 has undergone one complete rotation at the target angular velocity.

The inputs of the "Simulation" module are the geometric measures $\{x_1, x_2, x_3\}$, which determine the local coordinates of points Q, A, B, and O. Simulation outputs are all body and point coordinates and their derivatives, and all applied and constraint forces. Each of these quantities is a function of time.

3.2 Functionality Calculation. The following quantities are calculated based on the trajectory data received from the "simulation" module.

- The minimum and maximum gap over time between the cutting blade edges (functionality indices 1 and 5, respectively).
- The minimum gap over time between the cutting blade bodies (functionality index 2).
- The maximum value over time of the displacement in the longitudinal and vertical web direction between the web position and cutting blade position, which arises during the interaction of the web and cutting blades (functionality indices 3 and 4, respectively).
- The extent of the web cutter working space in the longitudinal and vertical direction of the web movement (functionality indices 6 and 7, respectively).

The processing of these indices with the aim of evaluating the system operation success is described in Sec. 3.4.

3.3 Load Calculation. The calculation of the load indices is performed in four steps:

1. Calculation of longitudinal and transversal cutting forces and cutting moments, yielding three measures per body, each depending on one spatial coordinate and time.
2. Calculation of normal and shear stresses, yielding two measures per body, each depending on two spatial coordinates and time.
3. Calculation of equivalent normal stresses, merging normal and shear stresses into one variable.
4. Calculation of maximum equivalent normal stresses over both spatial dimensions and time, yielding one scalar measure per body, which is used as load index.

Calculation of cutting forces and cutting moments is based on the rigid body assumption and Newton's second law. The following relations are used:

$$F_L(x,t) = -\int_0^x \ddot{s}_L \rho A d\tilde{x} + \sum_k F_k^{(L)} I_{[x_{Fk},l]}(x) \tag{3.1}$$

$$F_T(x,t) = -\int_0^x \ddot{s}_T \rho A d\tilde{x} + \sum_k F_k^{(T)} I_{[x_{Fk},l]}(x) \tag{3.2}$$

$$M(x,t) = -\int_0^x F_T(\tilde{x},t) d\tilde{x} + \sum_k M_k I_{[x_{Mk},l]}(x) \tag{3.3}$$

where, F_L, F_T, and M are the longitudinal cutting force, transversal cutting force, and cutting moment; $\ddot{s}_L$ and $\ddot{s}_T$ are the longitudinal and transversal beam element accelerations; $F_k^{(L)}$, $F_k^{(T)}$, and M_k are the longitudinal and transversal components of the k-th external force and the k-th external moment; x_{Fk} and x_{Mk} are the corresponding coordinates of application of these loads; ρ, A, and x are the density, cross sectional area, and length coordinate of the beam element; and $I_S(x)$ is a switch function, which is equal to one if $x \in S$ and zero otherwise.[2]

Normal and shear stresses are calculated based on the cutting measures [25]. For the determination of equivalent normal stresses, denoted as $\bar{\sigma}_i(x,y,t)$, the distortion energy hypothesis is employed [26]. The load indices $\bar{\sigma}_{\max,i}$ are calculated as follows:

$$\bar{\sigma}_{\max,i} = \max_{[x,y,t]} \bar{\sigma}_i(x,y,t), \quad i = 1, \ldots, 5 \tag{3.4}$$

3.4 Performance Evaluation. The overall system performance is classified as unacceptable (failure) if the load and functionality indices, received from the corresponding modules, indicate the occurrence of at least one of the following events.

- Failure events 1–5: One of the received load indices (the maximum equivalent normal stress of a system component over space and time) is greater than the associated predefined maximum allowed normal stress. Occurrence of such event corresponds to system failure due to overstressing.
- Failure event 6: The minimum gap (over all time) between the cutting blade edges (functionality index 1) is greater than a predefined value. Occurrence of this event corresponds to web cutter malfunction because of its inability to successfully perform the cutting task as a result of the cutting blade edges remaining too far apart at all times.
- Failure event 7: The minimum gap (over all time) between the cutting blade bodies (functionality index 2) is negative. This event corresponds to the intrusion of the cutting blades.
- Failure events 8 and 9: The maximum longitudinal or vertical web displacement during cutting (functionality indices 3 and 4) is greater than an associated predefined maximum value. Occurrence of one of these events corresponds to web cutter malfunction because the movement of the web is too strongly disturbed by the cutting blades while cutting is performed.
- Failure events 10–12: The maximum gap between the cutting blade edges (functionality index 5), the working space in longitudinal web direction (functionality index 6), or the working space in the vertical web direction (functionality index 7) is greater than an associated predefined maximum value. Occurrence of one of these events corresponds to an inappropriate shape of the web cutter, violating demands on its compactness.

Evaluation of the above events requires the feasible ranges of all functionality indices to be provided a priori as constants of the performance evaluation module. If none of the above cases is found to be true, the system performance is classified as acceptable.

3.5 Estimation of Probability of Failure. MCS-based estimation of the probability of failure, as described in Sec. 2.4, requires the joint PDF of the dimensions $\mathbf{x}=[x_1 \;\; x_2 \;\; x_3]^T$, as well as another PDF, the biasing function. Both PDFs are constrained by the nominal values $\mathbf{x_n}=[x_1^{(n)} \;\; x_2^{(n)} \;\; x_3^{(n)}]^T$ (which determine the marginal means) and the tolerances $\mathbf{t}=[t_1 \;\; t_2 \;\; t_3]^T$ (which determine the marginal variances and bounds). Each dimension x_i ($i=1,2,3$) is assumed to be statistically independent and to be associated to a marginal PDF, which is a truncated Gaussian. An example of such PDF is displayed in Fig. 8. Truncation corresponds to the fact that if tolerances are not met during manufacturing, the corresponding component is discarded. The actual joint

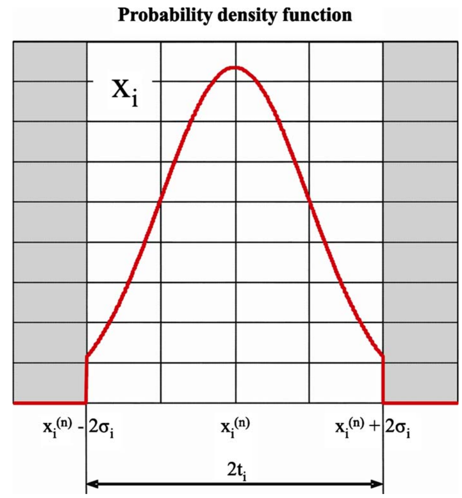

Fig. 8 Assumed real world marginal PDF of a geometric measure x_i

PDF of the dimensions is obtained by multiplying all marginal PDFs. The biasing function is chosen as a joint uniform distribution over the space of allowed dimensions. In our study, MCS are performed in packets of 10^5 samples.

3.6 Optimization of Nominal Measures and Tolerances. The following explicit mathematical relation is employed for the calculation of tolerance-related manufacturing costs of the web cutter mechanism:

$$C(\mathbf{t}) = \sum_{k=1}^{3} \frac{c_k}{t_k}, \quad c_k = 1 \quad \forall\, k \tag{3.5}$$

This relation has been freely chosen. The influence of nominal values on the overall manufacturing costs is neglected.

In order to obtain optimal tolerance assignments, the following optimization problem is solved by means of sequential quadratic programming (SQP):

$$\begin{aligned}
&\min_{\mathbf{x_n},\mathbf{t}} \quad C(\mathbf{t})\\
&\text{s.t.} \quad \beta_{\text{target}} - \beta_{\text{SVR}}(\mathbf{x_n},\mathbf{t}) \le 0\\
&\qquad x_{1,tl}^{(n)} \le x_1^{(n)} \le x_{1,tu}^{(n)} \quad t_{1,tl} \le t_1 \le t_{1,tu}\\
&\qquad x_{2,tl}^{(n)} \le x_2^{(n)} \le x_{2,tu}^{(n)} \quad t_{2,tl} \le t_2 \le t_{2,tu}\\
&\qquad x_{3,tl}^{(n)} \le x_3^{(n)} \le x_{3,tu}^{(n)} \quad t_{3,tl} \le t_3 \le t_{3,tu}
\end{aligned} \tag{3.6}$$

In this problem statement, $\beta_{\text{SVR}}(\mathbf{x_n},\mathbf{t})$ denotes the SVR-function that approximates the reliability index (see Sec. 2.5) and β_{target} denotes the target reliability index, which corresponds to a probability of failure of $p_{f,\text{target}}=\Phi(-\beta_{\text{target}})$, where Φ is the standard normal cumulative density function. The lower and upper bounds of the optimization variables $\mathbf{x_n}$ and $\mathbf{t}$, denoted as $x_{1,tl}^{(n)}$, $x_{1,tu}^{(n)}$, $x_{2,tl}^{(n)}$, $x_{2,tu}^{(n)}$, $x_{3,tl}^{(n)}$, $x_{3,tu}^{(n)}$, $t_{1,tl}$, $t_{1,tu}$, $t_{2,tl}$, $t_{2,tu}$, $t_{3,tl}$, and $t_{3,tu}$, are equal to the limits of the regression function domain.

4 Results

In order to get an insight into the decomposition of the space of random geometric measures of the web cutter and to quantify the accuracy of the SVM-based approximation of the limit state function, a very large set of reference data was created. This set consisted of a uniform three-dimensional grid, comprising $55^3 = 166{,}375$ sample geometric realizations, which were generated over the following intervals:

[2]As an alternative to calculating the cutting measures analytically, they can be calculated numerically during simulation. To accomplish that, a rigid joint can be introduced for each body and, at each time step, shifted over the whole body length. The cutting measures can then be found as the joint-related reaction forces and moments, emerging at each considered joint position.

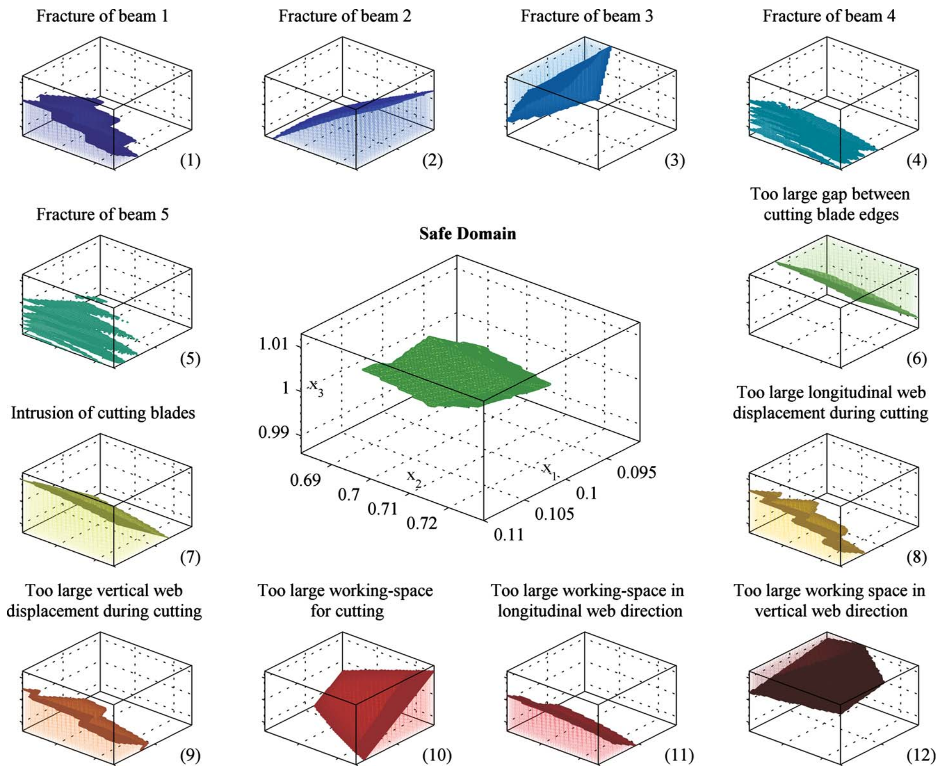

Fig. 9 Configuration space, spanned by uncertain geometric measures x_1, x_2, and x_3. Domains associated to each failure event (Subfigs. 1–12) and overall safe domain.

$$0.091 \le x_1 \le 0.11, \quad 0.682 \le x_2 \le 0.729, \quad 0.986 \le x_3 \le 1.013$$

Each sample was analyzed via multibody simulation (Secs. 2.1 and 3.1–3.4; note that it should be emphasized at this point that this large number of function calls is just for the purpose of comparison, and that the actual approach uses far less samples, as described subsequently). The regions in the space of uncertain geometric measures that are associated to the failure events described in Sec. 3.4, and the resulting exact overall safe domain are presented in Fig. 9. Some of the failure domains are found to be nearly linear (Subfigs. 2, 6, 7, and 10), while some are highly nonlinear (Subfigs. 1, 4, 5, 8, and 9). The "global" limit state function, boundary of the overall safe domain (depicted in the central subfigure), comes out to be a highly nonlinear closed surface in the space of random geometric measures. This domain is characterized by sharp edges (discontinuities in the first partial derivatives).

An SVM-based approximation of the limit state (Sec. 2.2) was obtained using 178 sample realizations of the uncertain geometric measures. The ranges of these measures are:

$$0.091 \le x_1 \le 0.11, \quad 0.682 \le x_2 \le 0.729, \quad 0.986 \le x_3 \le 1.013$$

An initial set of 40 samples was distributed uniformly over the considered space. The remaining samples were chosen adaptively (Sec. 2.3). The width parameter of the Gaussian kernel used was updated after the addition of each new sample, as mentioned in Sec. 2.3. A width parameter of 0.1 was used to construct the final SVM limit state function (Fig. 10). In the figure, the large dots represent the samples used for the training of the SVM-function. The small dots represent all samples of the large reference data set, which were falsely classified by the SVM, thus providing a "measure" of the error of the approximated limit state function.

It is noticeable that the adaptive sampling scheme successfully yielded an increased sampling density in the vicinity of the limit state while avoiding clustering effects. Hence, each sample was characterized by a high content of unique information about the location of the limit state. Reclassification of the samples of the reference data set using the SVM-function yielded a correct reclassification rate of 96.6%.

In order to define an appropriate domain for the regression of the reliability index (Secs. 2.4, 2.5, and 3.5), 150,000 sample nominal values of the uncertain geometric measures of the web cutter and corresponding tolerances were distributed over the (six-dimensional) subspace with the following bounds:

$$0.093 \le x_1^{(n)} \le 0.109, \quad 0.688 \le x_2^{(n)} \le 0.725,$$

$$0.991 \le x_3^{(n)} \le 1.01$$

$$10^{-5} \le t_1 \le 0.016, \quad 10^{-5} \le t_2 \le 0.037, \quad 10^{-5} \le t_3 \le 0.019$$

The samples were analyzed by means of MCS, employing the previously generated SVM-function (note that there is no actual simulation call at this point but simply SVM evaluations). All samples whose associated reliability indices were located between $-\infty$ and 2.8 ($\Leftrightarrow p_f \in (2.56 \cdot 10^{-3}, 1)$) or between 5 and ∞ ($\Leftrightarrow p_f \in (0, 2.86 \cdot 10^{-7})$) were discarded. The minimum and maximum coordinate values of the remaining samples were selected as the limits of the regression function domain:

$$0.095 \le x_1^{(n)} \le 0.098, \quad 0.69 \le x_2^{(n)} \le 0.7, \quad 0.991 \le x_3^{(n)} \le 0.997$$

$$1.3 \cdot 10^{-5} \le t_1 \le 332.3 \cdot 10^{-5},$$

$$3.3 \cdot 10^{-5} \le t_2 \le 987.7 \cdot 10^{-5}, \quad 6.3 \cdot 10^{-5} \le t_3 \le 609.9 \cdot 10^{-5}$$

Two sets of samples stemming from that region were generated by means of CVT: a training set comprising 1000 samples and a testing set comprising 5000 samples. The probabilities of failure and the corresponding reliability indices were calculated using MCS for all these samples. The training set was used for the generation of the regression function by means of SVR. The regression function accuracy was assessed based on the testing set.

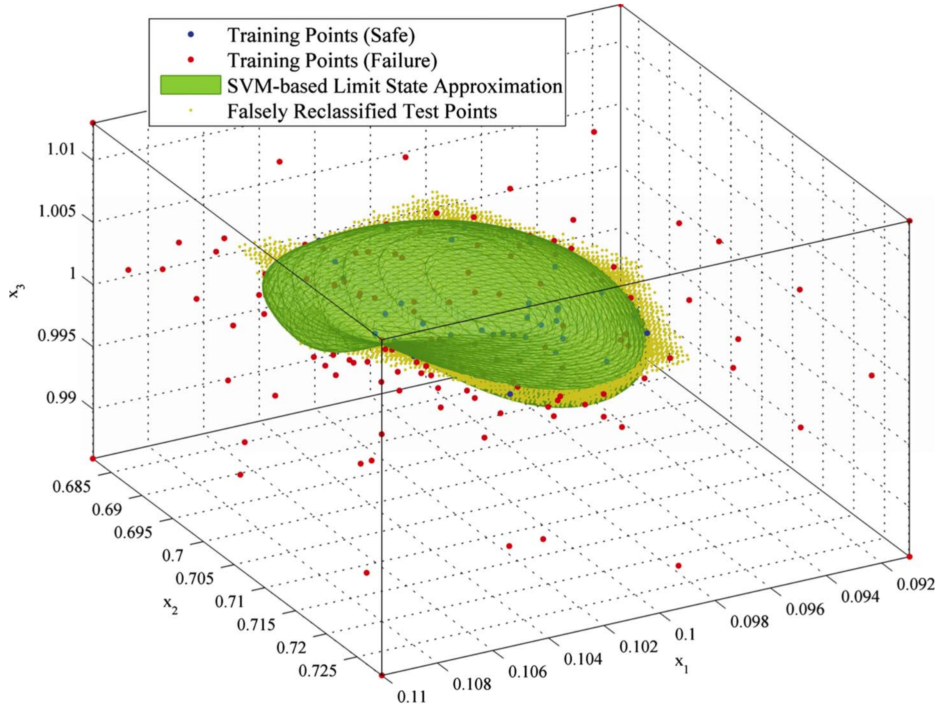

Fig. 10 SVM-based approximation of the limit state (meshed surface), samples used for training of the SVM-function (large dots), and samples of the reference data set, which were falsely reclassified based on the SVM-function (small dots)

Reevaluation of the testing samples of the region of interest using the SVR-function yielded a mean absolute difference between MCS-based and SVR-function-based reliability index estimates of $\text{mean}_{(\mathbf{x_n},\mathbf{t})_{\text{Test}}}\{|\beta_{\text{MCS}}-\beta_{\text{SVR}}|\}=0.35$. In terms of the probability of failure, this difference corresponds to $\text{mean}_{(\mathbf{x_n},\mathbf{t})_{\text{Test}}}\{|p_{f,\text{MCS}}-p_{f,\text{SVR}}|\}=0.09\%$. The associated maximum values are $\max_{(\mathbf{x_n},\mathbf{t})_{\text{Test}}}\{|\beta_{\text{MCS}}-\beta_{\text{SVR}}|\}=1.38$ and $\max_{(\mathbf{x_n},\mathbf{t})_{\text{Test}}}\{|p_{f,\text{MCS}}-p_{f,\text{SVR}}|\}=1.06\%$, respectively.

Using the SVR-function, the RBDO problem (3.6) was solved based on SQP (Secs. 2.5 and 3.6) with an analytic evaluation of all Jacobians. A target reliability index of $\beta_{\text{target}}=3.29$ was chosen, which corresponds to a target probability of failure of $p_{f,\text{target}}=0.05\%$. As a start of the optimization, the center point of the space of considered nominal measures was used. Starting tolerances were defined as the minimum values considered. Starting nominal measures and starting tolerances formed a feasible point with no active constraints and a cost value of 21,735. After 38 SQP iterations, optimization converged to the following optimal solution:

$$\mathbf{x_n^{(opt)}}=\begin{bmatrix}9.83 & 69.85 & 99.73\end{bmatrix}^T\cdot 10^{-2}$$

$$\mathbf{t^{(opt)}}=\begin{bmatrix}2.4 & 4.78 & 3.17\end{bmatrix}^T\cdot 10^{-3}$$

For this solution, the probabilistic constraint is active; all other constraints are inactive. The cost at the solution is equal to 942. The distance between the starting and optimal point is equal to:

$$\mathbf{x_n^{(opt)}}-\mathbf{x_n^{(\text{Start})}}=\begin{bmatrix}1.7 & 3.3 & 3.1\end{bmatrix}^T\cdot 10^{-2}$$

$$\mathbf{t^{(opt)}}-\mathbf{t^{(\text{Start})}}=\begin{bmatrix}2.38 & 4.74 & 3.1\end{bmatrix}^T\cdot 10^{-3}$$

Multiple starting nominal measures were generated by spanning a grid of $6^3=216$ samples over the space of considered nominal measures. Optimization was reexecuted for each sample, each time yielding a convergence to the aforementioned solution.

For the sake of comparison, the actual reliability index associated to $\mathbf{x_n^{(opt)}}$ and $\mathbf{t^{(opt)}}$ was estimated by means of MCS and is equal to $\beta_{\text{MCS}}(\mathbf{x_n^{(opt)}},\mathbf{t^{(opt)}})=3.68$, which corresponds to a probability of failure of $p_{f,\text{MCS}}(\mathbf{x_n^{(opt)}},\mathbf{t^{(opt)}})=0.01\%$. Hence, the SVR-function yielded a conservative estimate of system reliability at $\mathbf{x_n^{(opt)}}$ and $\mathbf{t^{(opt)}}$.

The solution of the RBDO problem is depicted within the space of uncertain geometric measures (Fig. 11). The large dot (at the intersection point of the lines) represents the optimal nominal geometric configuration $\mathbf{x_n^{(opt)}}$. The rectangles represent the associated optimal tolerance assignments $\mathbf{t^{(opt)}}$. The outer surface, serving as a reference, indicates the SVM-based limit state approximation. The inner surface gives an impression of the real world distribution of geometric measures $\boldsymbol{x}_i (i=1,2,3)$, which results from the RBDO solution. It is an isosurface of the joint PDF $f_{\mathbf{X}}(\mathbf{x};\mathbf{x_n^{(opt)}},\mathbf{t^{(opt)}})$, which encloses 90% of all possible geometric outcomes.

5 Conclusion

This study describes a novel method to perform a reliability-based design and tolerance optimization for multibody systems. The core of this approach is based on the notion of explicit design space decomposition, whereby the boundary of the failure domain is constructed explicitly using an SVM. SVM-based explicit limit state functions enable an efficient calculation of probability of failure, as well as an efficient adaptive sampling for the reduction in the number of function evaluations. The probabilistic constraint of an RBDO problem can subsequently be replaced by an approximation allowing the problem to be solved efficiently. The approach, which was applied to a web cutter, can handle an arbitrary number of failure modes, arbitrary probabilistic distributions of the uncertain variables, discontinuous system responses, and nonlinear and disjoint limit states. It can be automated to a large extent and can provide the designer with more insight into complex system dependencies such as an explicit knowledge of where the failure regions are.

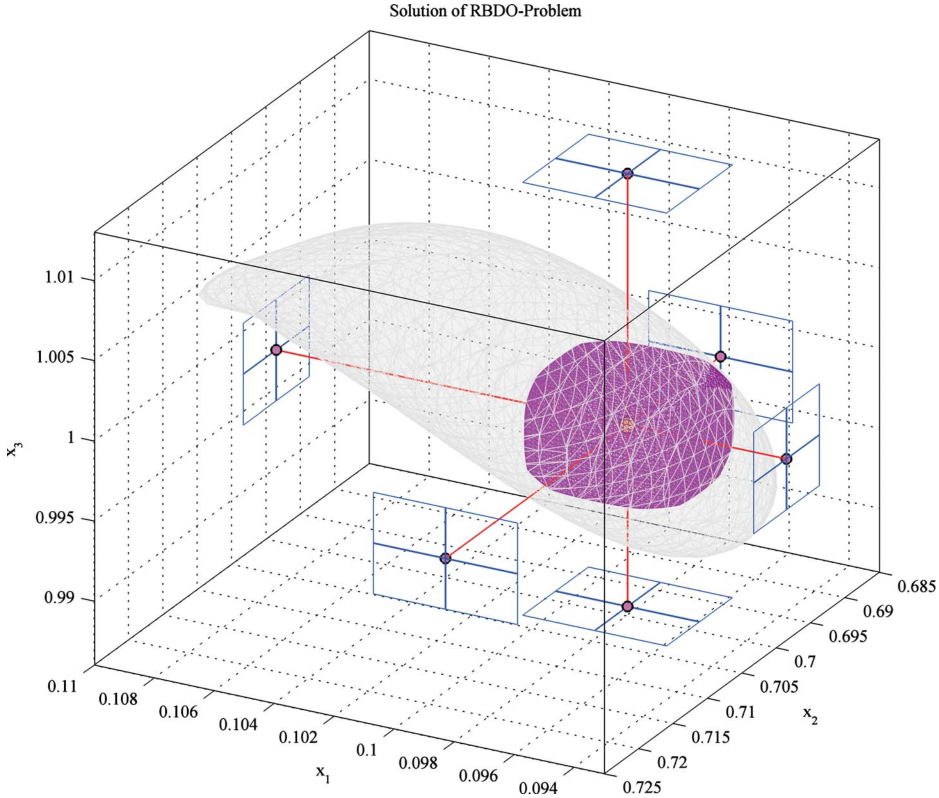

Fig. 11 Optimal nominal measures (dot at intersection of lines) and associated optimal tolerances (represented by rectangles) of the web cutter mechanism. Outer surface: SVM-based approximation of the limit state. Inner surface: isosurface of the joint probability density function of a geometric system outcome, which corresponds to a constant function value of 7.01×10^{-4}.

The methodology has been shown to be computationally feasible in the case of three uncertain variables. Local errors of the design space decomposition occur mainly in the vicinity of the boundaries. Such errors would require some degree of conservativeness (e.g., a reduction in the safe region volume) if a real world application is tackled.

Subsequent work will focus on investigating the efficiency of the proposed approach for larger scale multibody systems with more geometric properties and tolerance intervals. Also, the accuracy of the design space decomposition will be increased further by improving the convergence properties of the adaptive sampling scheme.

Probabilistic SVMs will be introduced, which map the distance between a sample and the optimal hyperplane to the confidence of classification as “safe.” This allows for an easy assessment of the expected accuracy of an SVM model and, more importantly, a customization of the degree of conservativeness of the methodology. The latter is achieved by associating the limit state, not to the nominal confidence level of 50%, but to a higher confidence level of choice (e.g., 99%), meaning that the safe region is composed of reliably safe configurations only. A change in the target confidence level does not require retraining of the SVM-function. It is therefore feasible to generate a series of solutions, each one associated to a different degree of conservativeness.

In order to apply the proposed methodology in practice, a user-optimized design tool can be developed, which automates design space decomposition, MCS, and probability of failure regression and optimization, leaving only the nominal classification algorithm (i.e., the algorithm for modeling- and simulation-based classification of an arbitrary outcome of the uncertain system variables as either safe or “failure”) and the probabilistic distributions of the uncertain variables to be provided by the user.

Acknowledgment

The support of the National Science Foundation (Grant No. CMMI-0800117) is gratefully acknowledged.

Nomenclature

$\mathbf{x}$ = vector of uncertain geometric measures, $\mathbf{x}=[x_1\ \ x_2\ \ x_3]^T$

$\mathbf{x_n}$ = vector of nominal values of $\mathbf{x}$, $\mathbf{x_n}=[x_1^{(n)}\ \ x_2^{(n)}\ \ x_3^{(n)}]^T$

$\mathbf{t}$ = vector of tolerances of $\mathbf{x}$, $\mathbf{t}=[t_1\ \ t_2\ \ t_3]^T$

p_f = probability of failure, $p_f=p_f(\mathbf{x_n},\mathbf{t})$

β = reliability index, $\beta=-\Phi^{-1}(p_f)$

References

[1] Huang, Y. M., and Shiau, C. S., 2006, “Optimum Tolerance Allocation for a Sliding Vane Compressor,” ASME J. Mech. Des., **128**(1), pp. 98–107.

[2] Caro, S., Bennis, F., and Wenger, P., 2005, “Tolerance Synthesis of Mechanisms: A Robust Design Approach,” ASME J. Mech. Des., **127**(1), pp. 86–94.

[3] Myers, R. H., and Montgomery, D. C., 2002, *Response Surface Methodology*, 2nd ed., Wiley, New York.

[4] Wang, G., and Shan, S., 2007, “Review of Metamodeling Techniques in Support of Engineering Design Optimization,” ASME J. Mech. Des., **129**(4), pp. 370–380.

[5] Haldar, A., and Mahadevan, S., 2000, *Probability, Reliability, and Statistical Methods in Engineering Design*, Wiley, New York.

[6] Ghanem, R., and Spanos, P. D., 1991, *Stochastic Finite Elements: A Spectral Approach*, Springer, New York.

[7] Kharmanda, G., Mohamed, A., and Lemaire, M., 2002, “Efficient Reliability Based Design Optimization Using a Hybrid Space With Application to Finite Element Analysis,” Struct. Multidiscip. Optim., **24**, pp. 233–245.

[8] Youn, B. D., and Choi, K. K., 2004, “Selecting Probabilistic Approaches for Reliability Based Design Optimization,” AIAA J., **42**(1), pp. 124–131.

[9] Adams, B. A., Eldred, M. S., and Wittwer, J. W., 2006, “Reliability Based Design Optimization for Shape Design of Compliant Micro-Electro-Mechanical Systems,” *Proceedings of the 11th AIAA/ISSMO Symposium on Multidisciplinary Analysis and Optimization*, Portsmouth, VA.

[10] Trosset, M. W., Alexandrov, N. M., and Watson, L. T., 2003, "New Methods for Robust Design Using Computer Experiments," *Proceedings of the Section on Physical and Engineering Sciences*, American Statistical Association.
[11] Burges, C. J. C., 1998, "A Tutorial on Support Vector Machines for Pattern Recognition," Data Min. Knowl. Discov., **2**(2), pp. 121–67.
[12] Romero, V. J., Burkardt, J. V., Gunzburger, M. D., and Peterson, J. S., 2006, "Comparison of Pure and Latinized Centroidal Voronoi Tesselation Against Various Other Statistical Sampling Methods," Reliab. Eng. Syst. Saf., **91**, pp. 1266–80.
[13] Beachkofski, B. K., and Grandhi, R., 2002, "Improved Distributed Hypercube Sampling," AIAA Paper No. AIAA-2002-1274.
[14] Basudhar, A., and Missoum, S., 2008, "Adaptive Explicit Decision Functions for Probabilistic Design and Optimization Using Support Vector Machines," Comput. Struct., **86**(19–20), pp. 1904–1917.
[15] Basudhar, A., and Missoum, S., 2008, "Two Alternative Schemes to Update SVM Approximations for the Identification of Explicit Decision Functions," *Proceedings of the 12th AIAA/ISSMO Multidisciplinary Analysis and Optimization Conference*, Victoria, BC, Canada.
[16] Missoum, S., Ramu, P., and Haftka, R. T., 2007, "A Convex Hull Approach for the Reliability-Based Design of Transient Dynamic Problems," Comput. Methods Appl. Mech. Eng., **196**, pp. 2895–2906.
[17] Missoum, S., 2007, "Controlling Structural Failure Modes During an Impact in the Presence of Uncertainties," Struct. Multidiscip. Optim., **34**(6), pp. 463–472.
[18] Basudhar, A., Missoum, S., and Harrison Sanchez, A., 2008, "Limit State Function Identification Using Support Vector Machines for Discontinuous Responses and Disjoint Failure Domains," Probab. Eng. Mech., **23**(1), pp. 1–11.
[19] Cristianini, N., and Schölkopf, B., 2002, "Support Vector Machines and Kernel Methods: The New Generation of Learning Machines," AI Mag., **23**(3), pp. 31–41.
[20] Shawe-Taylor, J., and Cristianini, N., 2004, *Kernel Methods for Pattern Analysis*, Cambridge University Press, Cambridge, England.
[21] Gunn, S. R., 1998, "Support Vector Machines for Classification and Regression," Technical Report No. ISIS-1-98, Department of Electronics and Computer Science, University of Southampton.
[22] Youn, B. D., Choi, K. K., and Du, L. L., 2005, "Adaptive Probability Analysis Using an Enhanced Hybrid Mean Value Method," Struct. Multidiscip. Optim., **29**, pp. 134–148.
[23] Smola, A. J., and Schoelkopf, B., 2004, "A Tutorial on Support Vector Regression," Stat. Comput., **14**, pp. 199–222.
[24] Nikravesh, P. E., 2008, *Planar Multibody Dynamics: Formulation, Programming and Applications*, CRC, Boca Raton, FL.
[25] Gere, J., 2000, *Mechanics of Materials*, Brooks-Cole, Belmont, MA.
[26] Schnell, W., Gross, D., and Hauger, W., 2002, *Technische Mechanik*, Springer-Verlag, Berlin.